Materials Science Forum
ISSN: 1662-9752, Vol. 1130, pp 35-48
doi:10.4028/p-kCuq7j

Submitted: 2023-12-04
Revised: 2024-03-09
Accepted: 2024-03-18
Online: 2024-10-31

Effect of Homogenization Cycle on Precipitation of Dispersoids and Abnormal Grain Growth in an Al-Mg-Si Alloy

Sumit Kumar Gahlyan[1,a], Pankaj Shivaji Wanjari[1,b], Shavi Agrawal[2,c], Butchi Bharadwaj[1,d], Manu Saxena[1,e], Vivek Srivastava[1,f]

[1]Hindalco Innovation Centre-Semifab, Hindalco Industries Ltd, Plot no.2, Taloja MIDC, Navi Mumbai-410208, Maharashtra, India

[2]Materials Engineering, Indian Institute of Science, CV Raman Road, Bangaluru, Karnataka, 560012, India

[a]sumit.gahlyan@adityabirla.com, [b]pankaj.wanjari@adityabirla.com, [c]shaviagrawal@iisc.ac.in, [e]manu.saxena@adityabirla.com, [d]butchi.bharadwajc@adityabirla.com, [f]srivastava.v@gmail.com

Keywords: Dispersoids, Homogenisation heating rate, Peripheral Coarse Grain (PCG).

Abstract. AA6xxx alloys are used for various automotive and architectural applications where microstructural characteristics are critical to have acceptable final properties. Abnormal Grain Growth (AGG) in these alloys, industrially termed as Peripheral Coarse Grain (PCG) is undesirable and Mn, Cr based non-coherent dispersoids are used to control the extent of PCG. Homogenization soaking temperature and time along with heating rates determine the size, distribution with grains and volume fraction of these dispersoids. In this study the heating rates are varied in lab and industrial setting to assess the effect of aforementioned dispersoid features using SEM and digital microscopy. It is found that higher heating rates lead to coarser and lower area fraction of dispersoids which finally results in markedly large PCG in industrial extrusion. Observed dispersoid features were described based on basic kinetics and Thermo-CalcTM predicted trends of micro-segregation, fraction of dispersoids and fraction of potential nucleating sites (β'-Mg_2Si) of dispersoids. A static recrystallization model was used to calculate the driving and retarding pressures based on substructural (EBSD analysis) and dispersoid features (SEM+ image analysis). The predicted recrystallisation response and PCG grain size was in close agreement with the observed values. This study highlights the significance of homogenization heating rates in addition to soaking time and temperature for PCG control.

Introduction

AA6xxx or Al-Mg-Si based aluminium alloys are commercially preferred for extrusion products which are used for various automobile and architectural applications. Each of the processing steps starting from casting till the finishing operation influence the final mechanical, corrosion, and cosmetic properties. However, in the commercial production, some of the processing steps maybe compromised to reduce costs without significantly affecting the final properties. Homogenisation, although a critical step in extrusion process is energy intensive, and it is always desirable to reduce the processing time here. Hence there is a strong motive to make the homogenisation heating rates faster. However, moving beyond a certain heating rate may negatively impact the final properties since the microstructural features might change significantly.

Dispersoids,α-Alx(MnFeCr)y,Si type, are important microstructural features in AA6xxx alloys for grain size control which are sensitive to heating rates and the heating rate may affect their distribution within grains [1,2,3,4,5,6]. It has been observed previously that the grain centres start to have lower number density of dispersoids with increased heating rates which has been related to presence of micro-segregation in the as cast microstructure. Nucleation of these non-coherent dispersoids is reported to occur heterogeneously either on β'-Mg_2Si [3,7] or u' [8] phases which is dependent on super-saturation of solutes and hence on micro-segregation. Dispersoids size and content significantly influence the deformation [9], dynamic recovery [10] and grain boundary mobility which are critical factors for control of recrystallisation and abnormal grain growth [11,12].

Corresponding to high strain, strain rates and high temperatures at extrudate surface, formation of Abnormal Grain Growth or as is commonly termed Peripheral Coarse Grain (PCG) is a known phenomenon and AA6xxx alloys are especially prone to these defects. In case of these alloys, static recrystallisation occurs as the extrudate exits the die, followed by Abnormal Grain Growth forming layer of coarse grains [13,14,15]. Variety of factors affect the formation and extent of PCG viz. extrusion ratio, container temperature, billet temperatures, die designs, cooling rate post extrusion and the microstructural features of billet [12,1,17,18]. Among these features, the role of dispersoids is critical for PCG control as has been described in aforementioned studies.

The effect of heating rate on segregation and with respect to that the role of final homogenisation temperature and time on final size, distribution, and fraction of dispersoids is described inadequately in literature. More importantly, the impact of heating rates, with industrial homogenisation trials, on dispersoids size, fraction, and subsequent formation of PCG is not documented. This paper attempts to do that through lab and industrial homogenisation trials followed by industrial extrusion trials. The dispersoid characteristics are explained in terms of the non-uniform distribution of nucleating sites of dispersoids on account of micro-segregation which is impacted by soaking temperature and time as well. The impact of heating rates on size and area fraction of dispersoids and consequently on PCG post extrusion is shown perhaps for the first time for an industrial production case. This study brings forth criticality of heating rate in addition to the soaking time and temperature for coarse grain control in an industrial setting.

Materials and Methods

A commercial AA6xxx series alloy was cast in a commercial Direct Chill (DC) caster in form of logs at Hindalco Industries Ltd, the nominal composition is tabulated in Table 1. To observe the effect of heating rate and soaking time on size, area fraction and distribution of dispersoids, samples from as cast condition were lab homogenised at two heating rates i.e., 120°C/hr (LS) and 200°C/hr (LF), and water quenched after soaking for a duration 3 and 9hrs at 540°C. Homogenisation trials were also conducted in continuous type industrial homogenisation furnace with two heating rates i.e., PS and PF such that heating rates were in following order PS<LS<LF<PF with soaking temperature of 540°C and soaking time of 9hrs. The homogenised billets of PS and PF condition were extruded in commercial production with an extrusion ratio of around 35 with an exit temperature of 470-500°C, water quenched after exiting the die.

Table 1. Nominal composition (wt%) of Al-Mg-Si alloy used for present investigation.

Elements	Si	Fe	Mn	Mg	Cu	Ti	Cr	Al
Wt %	0.72	0.17	0.39	0.87	0.35	0.017	0.017	Balance

To obtain representative sample of the logs, 20mm thick slices were cut in as cast and homogenised condition from the stable portion of the DC cast logs. For lab heat treatment simulations, 30x30mm samples were cut from the mid-radius of the log slices and homogenised in air circulating Carbolite furnace (HRF07045B). The samples for grain structure and EBSD were taken from the middle of extrudate in T5 condition. Routine metallographic preparation techniques were used to obtain mirror finish at sample surface for all the microscopic analyses. For grain structure imaging, polished samples were electro-etched in Barker's reagent in Struers Lectropol-5 at 25V for 220s. EDS analysis was carried on polished samples with Hitachi, S3400N fitted with Bruker EDS system. To perform EBSD analysis, mechanically polished samples were electro-polished in Struers A2 solution at 21V for 10s in Struers Letcropol-5. Imaging of dispersoids and EBSD mapping was carried in Gemini-400, Zeiss FEG-SEM with Oxford EBSD equipped with TSL8. The size and area fraction of dispersoids was estimated using *Fiji ImageJ* [19] by the method of thresholding the images. Segregation analyses was performed through Thermo-Calc 2023a [20] with TCAL5 database with built-in Scheil solidification model.

Result and Discussion

Micro-Segregation Analysis. As discussed in previous section, dispersoids formed during high heating rate homogenisation have inhomogeneous distribution from grain edges to centres. Elemental segregation in the as cast condition is a critical aspect that leads to dispersoid ±inhomogeneities and size differences within the grains. In the analysed as-cast sample, it is observed that there is significant amount of micro-segregation and absence of dispersoid (Fig.1) Colour contrast within grains and EDS mapping indicate local variations in elemental composition. In an industrial process, the cast logs are subsequently homogenised where one of the objectives is dispersoids precipitation. However, fast heating rate lead to low area fraction or absence of dispersoids towards grain centre and along the grain boundaries (Fig.2).

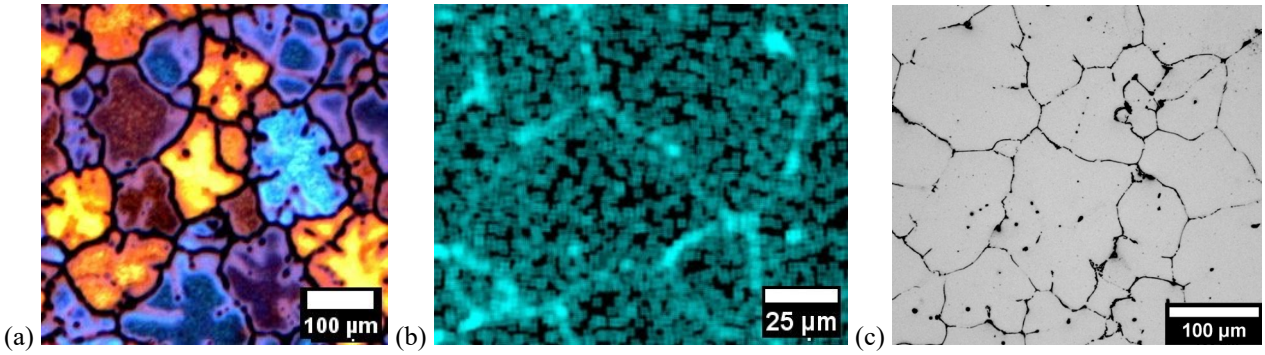

Fig. 1. As cast sample images in (a) Polarised light optical microscope; (b) Elemental SEM-EDS mapping showing Si segregation; (c) Digital microscope without any dispersoid precipitation.

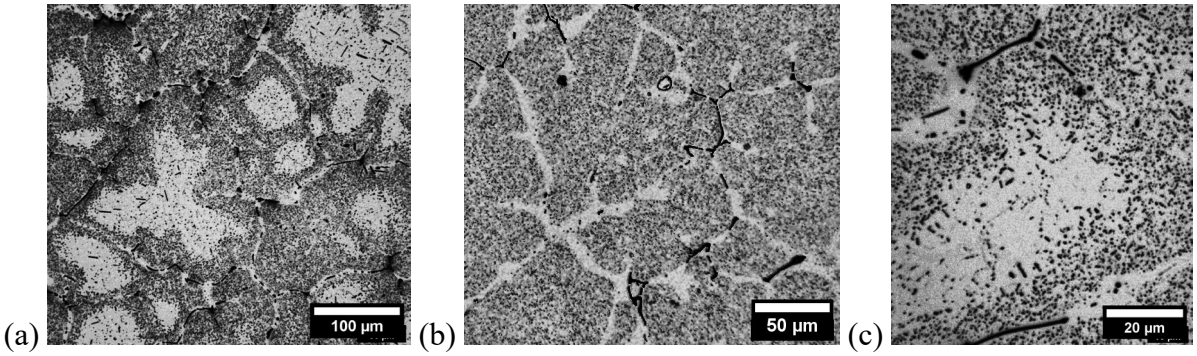

Fig. 2. Digital microscope image showing regions of lower dispersoid density (a) Grain centres (b) Along grain boundaries;(c) In a single grain (etched in 0.5%HF/15s).

Micro-segregation is the result of industrial DC casting where rapid solidification does not provide enough time for solute re-distribution. Solidification regime encountered in DC casting is closer to Scheil-Gulliver solidification [21] where the diffusion in solid is assumed to be zero and diffusion in liquid is assumed to be infinite. This solidification regime was used from Scheil module of Thermo-Calc to estimate the segregation encountered in DC casting.

To estimate the elemental segregation from grain centres to the grain boundaries, the concentration of each element in FCC was calculated as the solidification progressed in Scheil Module. Since solidification starts from grain centre (0.0R) and terminates at grain boundary (1.0R), solute content in FCC/Aluminium matrix at ≈100% liquid corresponds to the concentration at grain centre and solute content towards the end of solidification, ≈0% liquid corresponds to the concentrations close to grain boundary.

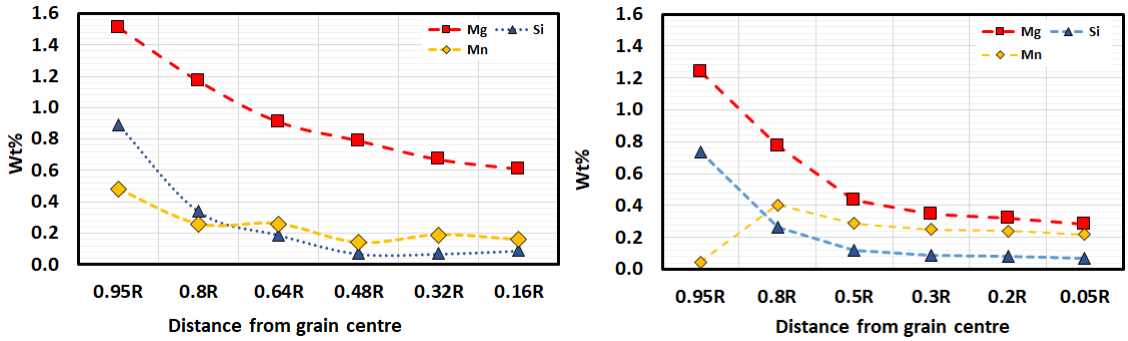

Fig. 3. Variation in solute concentration from grain centre (0R) towards the grain boundary (1.0R) obtained by (a) Scheil solidification, Thermo-Calc^{TM}; (b) SEM-EDX line profile

Considering this procedure in Thermo-Calc, the variation in solute content from grain edge towards the grain centre was calculated. This was compared with representative SEM-EDS line profile of one of the grains in as cast samples. It can be observed that the predictions follow the essential trend of SEM-EDS analysis (Fig.3). All the major alloying elements have a concentration gradient which is most prominent for Mg followed by Si and Mn. Mn concentration near 0.95D is tending to zero, this is due to partitioning of Mn to $Al_{15}Mn$ type intermetallics which are formed during solidification at grain boundaries. It could be expected that if these local variations in elemental compositions are not removed during homogenisation, it would influence subsequent dispersoid precipitation and lead to inhomogeneities.

Segregation Effect on β'-Mg_2Si and Dispersoid Precipitation. As mentioned previously, the nucleation of dispersoids is a heterogenous process and it occurs on β'-Mg_2Si or u' phase. Nucleation of u' phase is also reported to occur on β'-Mg_2Si [8] and hence uniform precipitation of β'-Mg_2Si is critical for subsequent uniformity of dispersoids. Precipitation of β'-Mg_2Si occurs through homogenous nucleation dependent on extent of Mg and Si supersaturation in the matrix. The temperature for precipitation and dissolution of β'-Mg_2Si is dependent on Mg and Si content and the phases formed prior to that and the temperature window of ≈200-400°C could be considered as important [22]. The dissolution occurs close to 350-450°C whereas the dispersoids precipitation would initiate at 400-450°C [8]. Conisdering the mentioned precipitation and dissolution processes at overlapping temperatures, the heating rates need to be estimated and adjusted accordingly. For example, the diffusion distance for Mg and Si (≈ $2*\sqrt{(Dt)}$ is 3-5µm for a duration of 1hr at 350°C and it would be even lower for lower temperature, hence the heating rates need to be slower in the initial ramp up from 200 to 350°C for uniform precipitation of β' phase [23].

However, during the industrial homogenisation processes, the heating rate may not be slow enough to remove segregation and have uniform β' precipitation. To demonstrate a case where the heating rate is such that the micro-segregation is not fully removed in the temperature range of β' precipitation, Thermo-Calc software is used for prediction of β' and dispersoids precipitation. Since β' and dispersoids precipitation is dependent on local elemental supersaturation, the equilibrium volume fraction of β'-Mg_2Si/dispersoids within regions of a grain could be estimated based on the local chemical composition. The local composition at few points were selected from the segregation profile of the Thermo-Calc results (Fig.3,a) for calculation of equilibrium β' and dispersoids volume fraction. The calculated results are plotted at 200°C and 300°C for β' and at 300°C for dispersoids precipitation (Fig.4)

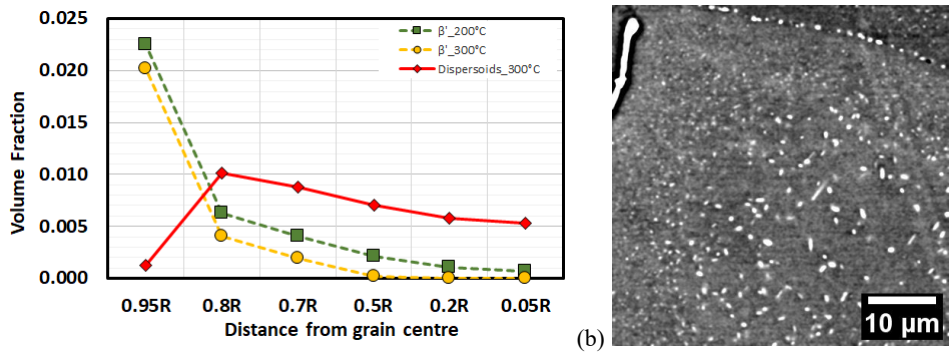

(a) (b)

Fig. 4. (a)Volume fraction of dispersoids and β'-Mg_2Si across the grain, calculated using Thermo-Calc (b) SEM image showing size and number area fraction variation across a grain in LF condition.

From the predicted results (Fig.4), it can be observed that the volume fraction of β'-Mg_2Si varied significantly from centre to edge implying that the nucleating sites for dispersoids will have similar trend and this non-homogeneity would be translated to dispersoids fraction. It is to be noted that the volume fraction calculated here is based on equilibrium conditions and kinetic consideration may change the fractions while the trends are expected to be retained. It could be observed that volume fraction of β'-Mg_2Si is almost zero near the grain centres and the nucleation sites thus would be of similar order. It is also observed that the volume fraction of dispersoids is not affected as severely as those of β'-Mg_2Si, hence the number of nucleation sites or number density of dispersoids would be affected more prominently compared to the volume fraction across the grains. This consideration therefore implies that in regions with low number of nucleating sites, the few dispersoids may grow to large sizes to achieve the desired volume fraction. These predictions are in line with the observations of high heating rate samples where the grain centre has very few but coarse dispersoids (Fig.4). The other important prediction is regarding the absence of dispersoids near grain boundaries which is a consequence of Mn segregation profile predicted earlier. This is in agreement to the absence of dispersoids adjacent to the grain boundaries, (Fig.2,b). The comments above need to be considered as qualitative since for quantitative predictions, more rigorous prediction tools and procedures would be needed.

Dispersoids Characterisation, Lab Schedule (LS, LF). In lab homogenised samples i.e., LS (120°C/hr) and LF (200°C/hr), the fraction and size of dispersoids at grain centres varied significantly from grain to grain within a single sample leading to significant scatter in image analysis. Considering this, image analysis for dispersoids characterisation was performed on images taken near the grain edges since the scatter within the samples was much less here. Based on the analysis (Fig.5,c), it could be observed that the median size of dispersoids in LS is higher than LF cycle for a soaking duration of 3hrs whereas for a duration of 9hrs the sizes were identical. The size of dispersoids increased in both the samples, however the change was more prominent in LF sample. The area fraction of dispersoids in LS is significantly lower than LF sample in case of 3hrs soak. With increased soaking time of 9hrs, the area fraction remained stable for LS sample whereas in case of LF, it reduced significantly up to 20% from 0.052 to 0.042.

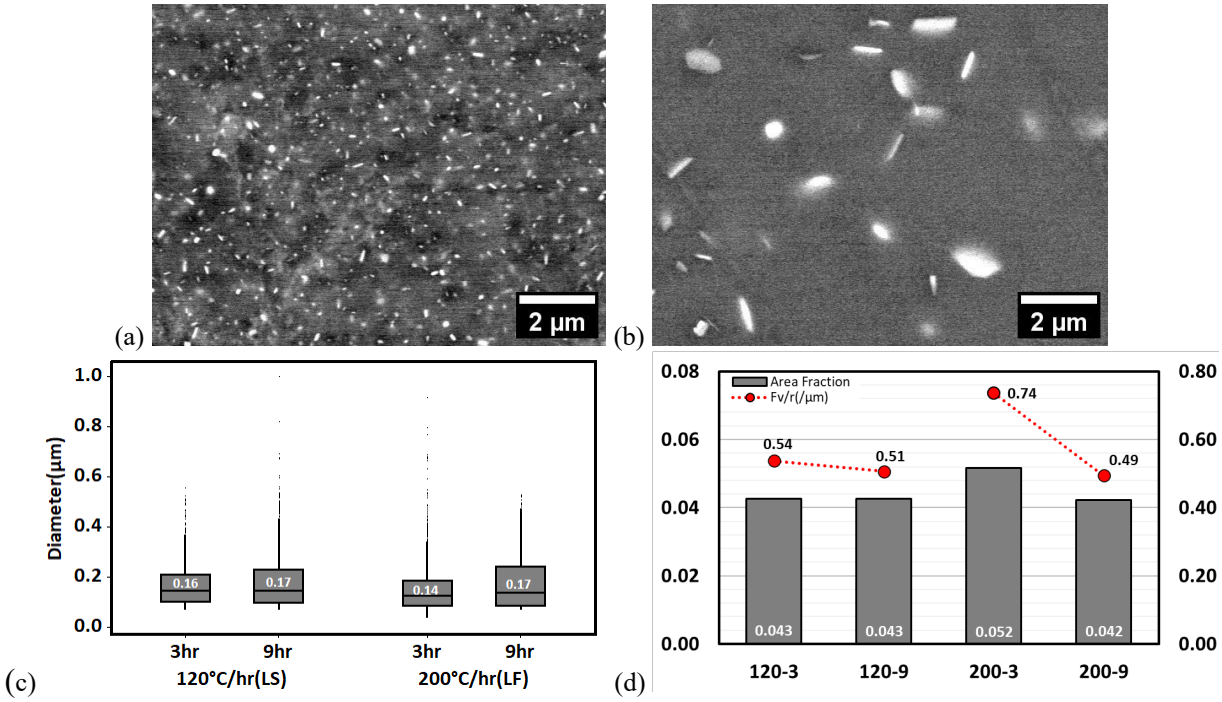

Fig. 5. SEM images of dispersoids for LF (200°C/hr) in region around (a) Grain edge, (b) Grain centre ; Plots of LS and LF for (c) Median dispersoid size (b) Area fraction (%) and Fv/r ratio(μm^{-1}).

In the temperature range of β' precipitation, at higher heating rates, segregation removal would be low since the diffusion distances are less for solute elements to redistribute. The grain boundaries have the highest supersaturation for Mg and Si atoms which can translate into higher number and volume fraction of nucleation sites and consequently higher number density and higher fraction of dispersoids. Therefore, this results in higher area fraction for faster heating rate (LF) compared to LS at 3hr soaking period.

At higher soaking time, the diffusion distances even for low diffusivity elements viz. Mn and Fe [23,24] becomes sufficient for long range diffusion. This would lead to significant reduction in local composition gradients, resulting in segregated zones attaining nominal composition across the grains. In this scenario the higher fraction of dispersoids precipitated out near the grain boundaries on account of higher supersaturations would also tend to move towards lowered equilibrium volume fractions as the soaking time increases. Hence, the volume fractions reduce near the grain boundaries and more prominently for the case where the initial segregations were high i.e., LF samples. Thus, for the fast-heating rate, LF there is a sharp drop in area fraction but the drop in LS is nominal indicating that at heating rate of LS, sufficient micro-segregation was removed. Similar area fractions for LS and LF at 9hrs soaking also indicate that the equilibrium area fraction for this alloy which would be ≈0.042 was achieved by LS in 3hrs soaking.

The coarsening of dispersoids on account of Gibbs-Thomson effect [21] is also observed for both rates and hence the dispersoid size is similar at 9hrs soaking. The initial difference in size of dispersoids between LS and LF samples could be explained by presence of higher number of nucleating sites in case of LF samples due to greater Mg and Si supersaturation. The gradient in volume fraction of β'-Mg_2Si is much higher than that of dispersoids (Fig.4,a). Thus, between LS and LF, when LF would retain higher segregation, the difference between number of nucleating sites would be higher than that of volume fraction of dispersoids. This would hence translate in finer dispersoid size at faster heating rate (LF) due to presence of higher number of nucleating sites per unit fraction of dispersoids. However, with increased soaking time, the finer dispersoids would dissolve due to coarsening and reduction in local equilibrium dispersoid volume as described previously. Thus, at 9hrs soaking time, the sizes in LS and LF become identical near grain boundaries as observed in these findings.

Dispersoids Characterisation, Plant Schedule (PS, PF). Subsequent to the lab homogenisation trials (LS, LF), to observe the effect of different heating rates on dispersoid evolution and consequently on coarse grain control, cast logs were homogenised in an industrial furnace (540°C-9hrs) with two heating rates as mentioned previously i.e., PF and PS. The logs were soaked for a duration of 9hrs instead of 3hrs, since F_v/r ratio (fraction of dispersoids/radius), didn't change significantly for LS samples, and additionally it was similar for both LF and LS samples. Higher soaking times are also preferred for better extrudability since AlFeSi intermetallics transform from β type to α type for longer soaking durations [25].

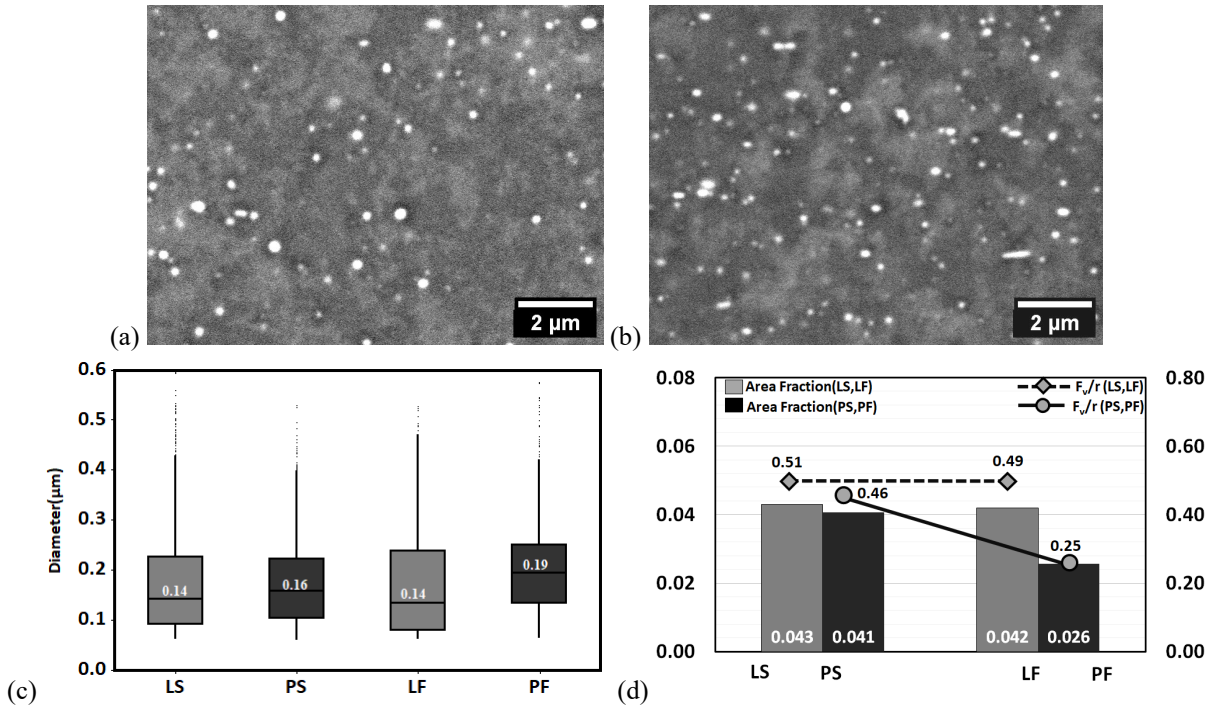

Fig. 6. SEM image of dispersoids in extruded samples processed with heating rate(a)PF (b) PS; Plots of LS, PS and PF, LF for (c) Median dispersoid size (b) Area fraction (%) and F_v/r ratio(μm^{-1}) for 540°C/9hrs homogenization.

The image analysis for these samples was done on cross section of extruded samples at locations 1mm from surface. The distance between two original grain boundaries reduces due to heavy deformation during extrusion and hence the analysed images of PS and PF represent dispersoid content averaged out over the radius of grains. The median dispersoids size in LS and LF samples was 0.17µm whereas the dispersoids in plant cycle PF is coarser i.e., 0.19µm and marginally finer i.e., 0.16 µm in PS. Higher size in PF could be explained from the fact that the in the analysis for PF sample, contribution of coarse dispersoids from grain centres is also accounted for as against the LS, LF samples where only regions near grain boundaries were examined. In case of PS sample, since the heating rates are slowest of all the examined cases, it would be expected that the coarsening at grain centres would be lower than any other case and it would shift the median size closer to LS median size.

However, the more critical difference is observed in case of area fractions wherein the area fraction of dispersoids in PF is almost 37% lower than that of PS samples. The measured area fraction in case of extruded (PS, PF) samples have contribution each from grain centres and grain edges as against the analysis of lab homogenised samples (LS, LF) where the fractions were determined only from the edges. At soaking time of 9hrs, as observed previously in LF sample, local equilibrium area fraction of dispersoids would be lowered and the dispersoids near the grain boundaries would gradually dissolve for the PF samples and hence the area fraction would be lowered near grain boundaries. PF is the highest heating rate in this study and hence the retention of concentration gradient would be highest for this case, also implying higher fraction of regions (grain centre) with lower number density of dispersoids and a greater number of such

grains (Fig.2,a). Additionally, at grain centres, no new dispersoids would nucleate since newer nucleating sites(β'/u') would not form at these temperatures. The effect of lowering of dispersoid fractions near the grain boundaries complemented with lower or no contribution of dispersoids towards grain centres would lead to significantly lower area fractions for PF samples. It follows that these effects would be accentuated with higher heating rates for a material with high micro-segregation and hence a remarkably low fraction of dispersoids is observed in case of PF sample as against PS sample. In case of PS, the area fraction is closer to LS samples as the heating rate is slowest of all cases and hence the degree of segregation would be marginal during precipitation of β'/u' and dispersoids. Thus, variation across grains would be minimal and increased soaking won't affect the area fraction of dispersoids.

PCG and Recrystallisation Model. The billets from each plant homogenisation schedule (PS, PF) were extruded with identical extrusion parameters followed by water quench at the press. Cross-section of the samples from the middle of the extrudate length were characterised for PCG using optical microscope. Faster heating rate (PF) led to formation of PCG which covered up to 50% of the rod surface where the size of grains ranged from 250μm to 2000 μm (Fig.7,b,d). In sharp contrast to that slower heating rate samples (PS) although subjected to same homogenisation soaking time and temperature restricted PCG levels up to 500μm from surface.

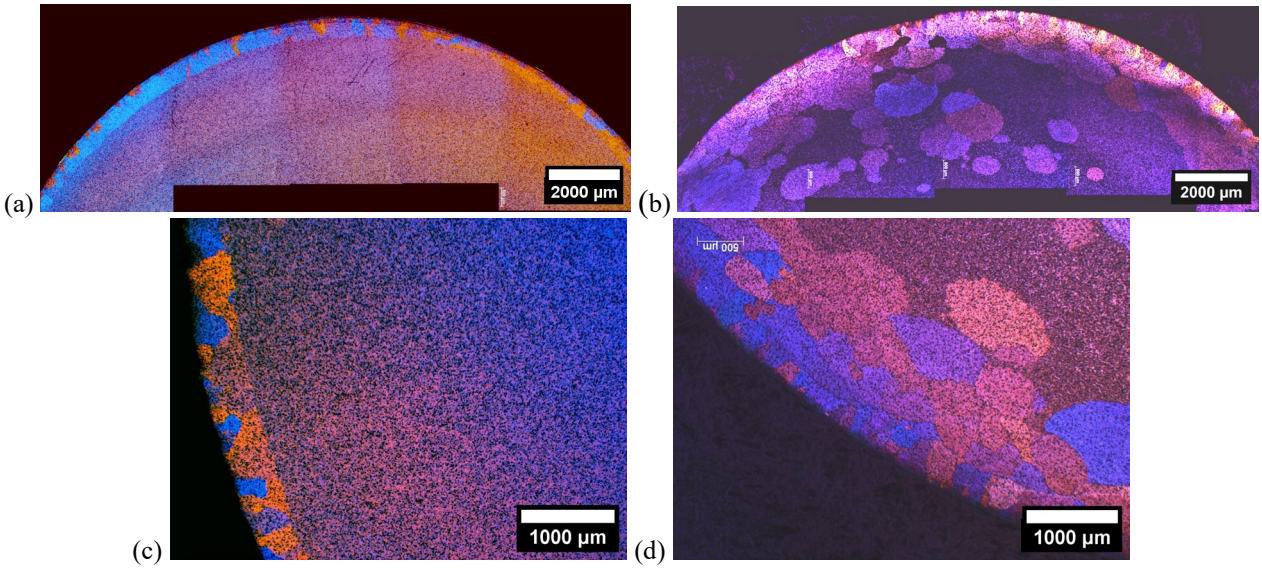

Fig. 7. Grain structure at cross-section of extrudate for billets processed with (a), (c) Plant slower heating rates, PS; (b),(d) Plant faster heating rate, PF.

For substructural examinations, EBSD mapping of the extrudate samples was performed on the cross section at ≈1mm from the surface. Because of heavy coarse graining in PF sample, only limited localised region with absence of PCG was observable and one of such regions was mapped at approx. 1mm from the surface.

The volume fraction of important micro-texture components were calculated through ATEX [26] with misorientation tolerance angle of 15°, it was observed that both samples had significant fraction of cube texture but none of the other important components were present, (Fig.8,a,b) in line with previous observation [27]. Grain boundary misorientation (MO) calculations showed that the fraction of High Angle Grain Boundaries (HAGB) i.e., boundaries with misorientation>15° was 37-43% whereas the Low Angle Grain Boundaries (LAGB), MO:1.5-5° was 36% in PF as against 26% in PS sample(Fig.8,c). Due to higher fraction of LAGB, PF sample has greater potential of static recrystallisation.

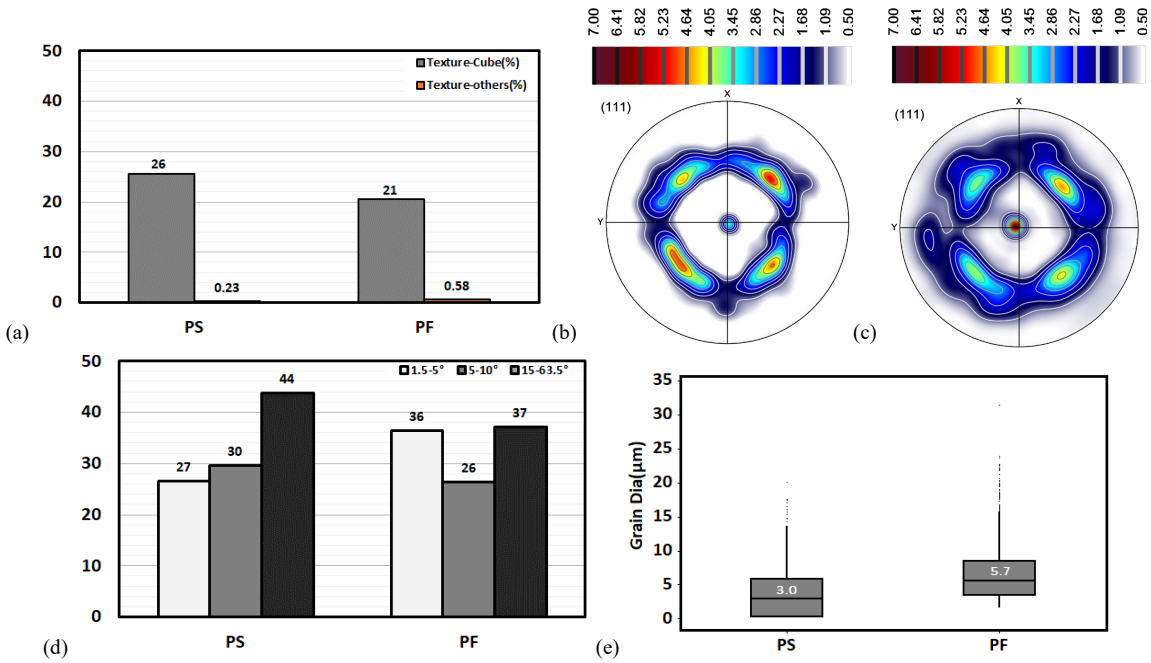

Fig. 8. Comparison of PS and PF samples in terms of (a) Micro-texture components (Cube & others); Pole figure derived from EBSD maps(b)PS(c)PF; (d)Grain boundary misorientation distribution; (e) Boxplot of subgrain size.

Higher degree of localised strains near the surface, accompanied by dynamic recovery processes may lead to progressive accumulation of dislocations at subgrain boundaries and hence increasing the boundary misorientation towards HAGB. This process is termed as Continuous Dynamic Recrystallisation (CDRX) [28,29] which may be accompanied by Geometric Dynamic Recrystallisation (GDRX). GDRX occurs when the preexisting grains are deformed to sizes closer to subgrain size and the grain boundary serrations eventually join to form HAGB subgrains. Both CRDX and GDRX have been reported as the mechanism of dynamic recrystallisation in extrusion conditions similar to here [14]. Since in recrystallisation process grains with HAGB grow to form strain free grains replacing LAGBs, the current microstructure has a potential for static recrystallisation which has previously been described for PCG mechanism [13,14,30]. Additionally, cube component in aluminium alloys is favourable for higher growth rates [31,32,33,34] which may aid in PCG.

The subgrain size was calculated considering the minimum grain size to be >0.6µm and grain tolerance angle to be 1.5° for both PS and PF samples. The minimum size and tolerance were fixed through multiple iterations of comparing subgrains from band contrast images with the calculated output grain images. The subgrain size distribution is different in PS and PF samples where the median subgrain size is 3.0 µm in PS samples as against 5.7µm in PF samples. Subgrains with larger size, highly mobile high angle grain boundary breakaway to form abnormally large grain during static recrystallisation where the cube grains growth is especially faster than other textures [33,34].

Due to dynamic recovery, it may be assumed that there would be no free dislocations inside the subgrains and the driving pressure for static recrystallisation would be provided by the dislocations from the subgrain boundaries. The driving pressure for this condition is described in Eq.1 [35] where γ_{SB} is subgrain boundary energy dependent on mean misorientation (θ) [36]. Here γ_{SB} is calculate based on Eq.2 where γ_m is the grain boundary energy associated with 15° misorientation(θ_m) i.e., 0.324J/m^2 [37] and mean misorientation, (MO<15°) between subgrains is calculated using EBSD. Subgrain size(δ) is dependent on Zener-Holloman parameter for an alloy [38], in this study it is the median subgrain size of PS(3.0µm), assuming no considerable coarsening has occurred here due to large pinning pressure of dispersoids and rapid water quench. This value is closer to previously reported value for a similar Al-Mg-Si system containing dispersoids [39], but slightly higher, probably due to lower extrusion ratio.

Counter acting to the driving pressure, non-coherent dispersoids provide retarding pressure through Zener pinning [40], Eq.3 where F_v is the area/volume fraction of dispersoids, and *r* is median dispersoid radius [41]. Additionally, on account of Gibbs-Thomson effect, grain curvature will also provide a retarding pressure, Eq.4 [30] where R and γ_{SB} are the radius and surface energy of recrystallising grain. Considering that highly misoriented and larger size grains would be potential recrystallising grains, surface energy associated with 15° grain boundary (0.324J/m^2) and 3rd quartile grain size (grain tolerance angle>15°) was selected for Eq.4.

$$P_D=3\gamma_{SB}/\delta \quad (1)$$

$$\gamma_{SB}=\gamma_m(\theta/\theta_m)(1-\ln(\theta/\theta_m)) \quad (2)$$

$$P_Z=\gamma_{GB}(3F_v/r) \quad (3)$$

$$P_C=2\gamma_m/R \quad (4)$$

$$P_{net}=P_D-P_Z-P_C \quad (5)$$

$$D_{rex}=v.t=(MP_{net}).t \quad (6)$$

Table 2. List of parameters/constants used for recrystallisation model.

Parameter/constant	PS	PF
Grain boundary energy,(HAGB), γ_{SB}	0.324J/m^2	0.324J/m^2
Subgrain size, δ	3.0μm	3.0μm
Mean misorientation, θ	7.4°	6.6°
Fraction of dispersoids, F_v	0.041	0.026
Median dispersoid size, r	0.16μm	0.19μm
3rd Quartile recrystallising grain radius, R	6.6μm	16.5μm
Time for static recrystallisation, t	15s	
Mobility of random orientation boundary(Al-1Mg) [42]	Mo: 367m^{4}J^{-1}s^{-1}; Q:170kJmol^{-1}	

Table 3. Driving, retarding pressures for recrystallisation and resultant grain size for PS, PF cycles.

	P_D (MPa)	P_Z (MPa)	P_C (MPa)	P_{net} (MPa)	Grain size (μm) Exit Temp: 450°C	Grain size (μm) Exit Temp: 490°C	Grain size (μm) Exit Temp: 510°C
PS	0.27	0.21	0.20	-0.13	NA	NA	NA
PF	0.26	0.10	0.08	0.08	225	990	2316

The net pressure for static recrystallisation would be determined by the difference of driving and retarding pressures for PS and PF cases, Eq.5. Using the values obtained from EBSD analysis (Table 2) and equations described above, the pressures were calculated as listed in Table 3. Due to markedly low fraction and higher size of dispersoids, Zener pinning pressure is almost halved in PF sample as compared to PS sample. Additionally, higher subgrain size distribution in PF sample provides lower retarding pressure from grain boundary curvature. Both these retarding contributions are higher in PF samples whereas the driving pressure was similar for both the cases. As a result, PS has a net negative pressure and hence no recrystallisation would be expected whereas in case of PF there is a net positive driving pressure suggesting potential for recrystallisation. To estimate the approximate size of recrystallised grain, the grain boundary velocity(v), is multiplied by quench delay time, t which was around 15s in this case. The velocity is calculated by taking the product of mobility of grain boundary and net driving pressure, Eq.6. Mobility of a random grain boundary is obtained here from the recrystallisation data of Al-1%Mg in [42] extrapolating to the typical exit temperature of 490°C.

The calculations predicted grain size around 1mm which is consistent with the size of coarse grains observed in PCG zone. It is to be noted that in this estimation, it is assumed that there is no impingement or restriction to the moving grain boundary from other recrystallising grains which would change when number of recrystallisation nucleation sites are very high, and in that case the final grain size could become much smaller. The actual grain boundary energies may be different and the subgrain size maybe lower since some degree of coarsening may have happened. Nevertheless, these calculations provide a good estimation of the order of recrystallised grain size and what could be expected in the given conditions. This study brings forth the significance of heating rate which impacts the Zener pinning, consequently subgrain coarsening and subsequent static recrystallisation leading to abnormal grain growth.

Summary and Conclusions

A range of homogenisation heating rates were studied in lab and plant conditions for evolution of dispersoids in Al-Mg-Si alloy in terms of size, area fraction and the distribution within grains. Non-uniform precipitation of dispersoids was observed within grains where grain centres had coarser and fewer precipitates and frequency of such regions increased with higher heating rates. This inhomogeneity was explained in terms of micro-segregation that occurs during industrial DC solidification, resulting in inhomogeneous precipitation of dispersoid nucleation sites i.e., u' or β'-Mg_2Si. Micro-segregation profile and precipitation of β'-Mg_2Si & dispersoids was predicted through Thermo-Calc which showed the precipitation trends observed in homogenised samples. Basis that, absence of dispersoids adjacent to the grain boundaries, absence or lower fraction towards grain centres, size evolution and changes in area fractions with changes in heating rates and soaking durations were explained.

To assess the effect of heating rates on final extrusion substructure and microstructure, two samples were subjected to varied heating rates in industrial homogenisation furnace (PS, PF) and extruded through industrial extrusion parameters. Although both PS and PF samples were homogenised at identical soaking temperature and time, the heating rate difference led to markedly large fraction of PCG in PF samples. The subgrain size and grain boundary misorientations analysed through EBSD were used in a static recrystallisation model. This model was used to demonstrate that reduction in Zener pinning pressure considering lower fraction and size of dispersoids and higher subgrain size in PF samples influenced the driving pressure for recrystallisation. Negative driving pressure in PS samples restricted the recrystallisation whereas positive driving pressure in PF aided by higher extrusion temperatures led to abnormal grain growth. The estimated grain size was close to observed size of coarse grains in PCG regions. The major takeaways could be listed down as below:

1. Micro-segregation in as cast material is retained at high heating rate homogenisation cycle leading to variation in dispersoids precipitation within the grains. It is observed that the number density of dispersoids reduce whereas the size of dispersoids increase from grain boundary to grain centre.
2. These variations could be explained by precipitation behaviour of dispersoid forming nucleating sites which are influenced by heating rates in the temperature range ≈200-400°C.
3. Compared to dispersoid size, the overall area fraction of dispersoids is affected more pronouncedly by heating rates.
4. The effect of heating rates is detrimental for PCG control in industrial settings even though the soaking time and temperature may be identical. The Zener pinning pressure is markedly reduced due to lower area fraction and higher dispersoid size at faster heating rates.
5. Based on microstructural features of extrudate, a static recrystallisation model could be used to estimate the final grain size in case of PCG formation.

The principles and modelling predictions used here for dispersoid feature evaluation may be used for prediction of dispersoids precipitation across grains in terms of size and number density with respect to various heating rates in future work. The recrystallisation model used here is basic and

could be used for initial estimation of coarse graining in AA6xxx alloys. To the best of our knowledge the combined impact of heating rates on dispersoid size, distribution and consequently on PCG has not been reported previously and this study brings forth this close and critical association which has great industrial significance.

Acknowledgements

I would like to thank Mahan team (Mr. Sanjay Chaturvedi and Mr. Deepak Khandelwal) for homogenisation trials and Renukoot team (Mr. Akhilesh Gupta, Mr. Rajan Deo) for the extrusion trials. I thank Dr Gautam Wagle for the review of manuscript and Prof. Satyam Suwas for providing the lab facilities at IISc, Bangalore.

References

[1] *The Effect of Heating Rate on the Density and Spatial Distribution of Dispersoids during Homogenisation of 6xxx Aluminium Alloys.* Magnus S. Remøe, Knut Marthinsen, Ida Westermann,Ketill Pedersen, Jostein Røyset and Oddvin Reiso. 2017, Materials Science Forum, Vol. 877, pp. 322-327.

[2] *Precipitation behavior of dispersoids in Al-Mg-Si-Cu-Mn-Cr alloy during homogenization annealing.* Yi Han, Ke Ma, Chuyan Wang, Hiromi Nagaumi. 2012. 13th International Conference on Aluminum Alloys (ICAA13). pp. 1817-1824.

[3] *Improved Distribution and Uniformity of a-Al(Mn,Cr)Si Dispersoids in Al-Mg-Si-Cu-Mn (6xxx) Alloys by Two-Step Homogenization.* Zhen Li, Jian Qin, Haitao Zhang, Xiaoguo Wang, Bo Zhang,and Hiromi Nagaumi. 2021, Metallurgical and Materials Transactions A, Vol. 52A, pp. 3204-3220.

[4] *The elemental distribution and precipitation kinetic of chromium dispersoids in Al-Mg-Si alloys.* M. Kenyon, J. Robson, J. Fellowes and Z. Liang. 2018. 16th International Aluminum Alloys Conference (ICAA16).

[5] *Characterization of the Density and Spatial Distribution of Dispersoids in Al-Mg-Si Alloys.* Magnus Sætersdal Remøe, IdaWestermann and Knut Marthinsen. 2019, Metals, Vol. 9, p. 26.

[6] *Dispersoid Precipitation and Process Modelling in Zirconium Containing Commercial Aluminium Alloys.* Prangnell, J. D. Robson and P. B. 2001, Acta Materialia, Vol. 49, pp. 599-613.

[7] *Precipitation process of AI-Mn and AI-Cr supersaturated solid solution in presence of age hardening phases.* Hirasawa, H. 1975, Scripta Metallurgica, Vol. 9, pp. 955-958.

[8] *Precipitation of dispersoids containing Mn and/or Cr in Al-Mg-Si alloys.* Lars Logaard, Nils Ryum. 2000, Materials Science and Engineering, Vol. 283, pp. 144–152.

[9] *The double-edge effect of second-phase particles on the recrystallization behaviour and associated mechanical properties of metallic materials.* Ke Huang, Knut Marthinsen, Qinglong Zhao, Roland E. Logé. 2018, Progress in Materials Science, Vol. 92, pp. 284-259.

[10] *The effect of dispersoids on the grain refinement mechanisms during deformation of aluminium alloys to ultra-high strains.* P.J. Apps, M. Berta, P.B Prangnell. 499-511, s.l. : Acta Materialia, 2005, Vol. 53.

[11] *Quantitative analysis of influence of α-Al(MnFeCr)Si dispersoids on hot deformation and microstructural evolution of Al−Mg−Si alloys.* Hiromi Nagaumi, Jian Qin, Cheng-bin Yu, Xiao-guo Wang, Lin-sheng Wang. 2022, Transactions of Non-Ferrous Scoiety of China, Vol. 32, pp. 1805-1821.

[12] *Effect of Dispersoids on the Microstructure Evolution in Al-Mg-Si Alloys.* Michael Kenyon, Joseph Robson, Jonathan Fellowes and Zeqin Liang. 2019, Advanced Engineering Materials, Vol. 21, p. 1800494.

[13] *Mechanism of the formation of peripheral coarse grain structure in hot extrusion of Al-4.5Zn-1Mg.* A. R. Eivani, J. Zhou & J. Duszczyk. 12, 2016, Philosophical Magazine, Vol. 96, pp. 1188-1196.

[14] *Surface grain structure development during indirect extrusion of 6xxx aluminium alloys.* W. H. Van Geertruyden, W. Z. Misiolek, P.T Wang. 2005, Journal of Materials Science, Vol. 40, pp. 3861-3863.

[15] *Evolution of Surface Recrystallization during Indirect Extrusion of 6xxx Aluminum Alloys.* W. H. Van Geertruyden, H. M. Browne, W. Z. Misiolek. 2005, METALLURGICAL AND MATERIALS TRANSACTIONS A, Vol. 36A, p. 1050.

[16] *The Effect of Die Bearing Geometry on Surface Recrystallization During Extrusion of an Al-Mg-Si-Mn Alloy.* Y. Mahmoodkhani, J. Chen, M.A. Wells, W.J. Poole, and N.C. Parson. 2019, METALLURGICAL AND MATERIALS TRANSACTIONS A, Vol. 50A, p. 5324.

[17] *Influence of different homogenization heat treatments on the microstructure and hot flow stress of the aluminum alloy AA6082.* Aurel Ramon Arnoldt, Andreas Schiffl, Heinz Werner Hoppel,Johannes Albert Osterreicher. 2022, Materials Characterization, Vol. 191, p. 112129.

[18] *Dispersoid Formation and Recrystallization Behavior.* Rong Hu, Tomo Ogura, Hiroyasu Tezuka, Tatsuo Sato and Qing Liu. 237-243, s.l. : J. Mater. Sci. Technol, 2010, Vol. 26(3).

[19] *Fiji: an open-source platform for biological-image analysis.* Schindelin, J., Arganda-Carreras, I., Frise, E. et al. 2012, Nature Methods, pp. 676-682.

[20] *Thermo-Calc Software.*

[21] David A. Porter, Kenneth E. Easterling, and Mohamed Y. Sherif. *Phase Transformations in Metals and Alloys.* Third. s.l. : CRC Press,Taylor & Francis Group, 2009.

[22] *The precipitation sequence in Al-Mg-Si alloys.* G. A. Edwards, K. Stiller, G. L. Dunlop and M. J. Couper. 11, 1998, Acta Metallurgica, Vol. 46, pp. 3893-3904.

[23] Gerhard Neaumann, Cornelis Tuijin. *Self-Diffusion and Impurity Diffusion in Pure Metals: Handbook of Experimental Data.* 1st . s.l. : Elsevier, 2009. ISBN: 978-1-85617-511-1.

[24] *A Unified Physical Model for Creep and Hot Working of Al-Mg Solid Solution Alloys.* Paoletti, Stefano Spigarelli and Chiara. 2018, Metals, Vol. 8, p. 9.

[25] Kuijper, Niels. Kinetics of the b-AlFeSi to a-Al(FeMn)Si transformation in Al-Mg-Si alloys. *Phd Thesis.* s.l. : Tu Delft, 2004.

[26] *Analysis tools for Electron and X-ray diffraction, ATEX software,.* Fundenberger, B. Beausir and J.J. s.l. : Université de Lorraine-Metz, France.

[27] *The Effect of the Extrusion Temperature on the Recrystallization Textures of an Extruded AA6005C Alloy.* Dr. Kentaro IHARA, Takahiro SHIKAMA, Keiji MORITA. 2013, 69 Kobelco Technology Review, Vol. 31, pp. 69-75.

[28] *Comportment mecanique et evolution structurale de l'aluminium au cours d'une deformation a chaud de grande amplitude.* Ch. Perdrix, M.Y. Perrin, F. Montheillet. 1981, Mém Et Sci Rev Métall, Vol. 78, p. 309.

[29] *An experimental study of the recrystallization mechanism during hot deformation of aluminium.* S. Gourdet, F. Montheillet. 2000, Materials Science and Engineering A, Vol. 283, pp. 274–288.

[30] F.J. Humphreys, M.Hatherly. *Recrystallisation and Related Annealing Phenomenon.* s.l. : Elsevier ltd., 2004.

[31] *Growth of cube grains during recrystallisation of aluminium.* E. Nes, J.K. Solberg. 1986, Material Science and Technology, Vol. 2, pp. 19-21.

[32] *The Cube Texture Revisited.* Hutchinson, Bevis. 2012, Materials Science Forum, Vols. 702-703, pp. 3-10.

[33] *Preferential Growth of Cube-Oriented Grains in Partially Annealed and Additionally Rolled Aluminum Foils for Capacitors.* Masakazu Kobayashi1, Yoshimasa Takayama and Hajime Kato. 12, 2004, Materials Transactions, Vol. 45, pp. 3247-3255.

[34] *Cube texture in hot-rolled aluminum alloy 1050 (AA1050)—nucleation and growth behavior.* Mohammed H. Alvi, S.W. Cheong, J.P. Suni, H. Weiland, A.D. Rollett. 2008, Acta Materialia, Vol. 56, pp. 3098-3108.

[35] *Dislocation models of crystal grain boundaries.* W.T. Read, W. Shockley. 3, 1950, Physical Review, Vol. 78, pp. 275-289.

[36] *Subgrain growth in heavily deformed Aluminium-Experimental Investigation and modelling treatment.* T Furu, R Orsund, E Nes. 6, 1995, Acta Materialia, Vol. 43, pp. 2209-2232.

[37] *Interfacial phenomena in metals and alloys.* Murr, L E. s.l. : Addison-Wesley Publishing Company, 1975.

[38] Sheppard, T. *Extrusion of Aluminium Alloys.* s.l. : Kluwer Academic Publishers, 1999.

[39] *Grain Structure Control of Flat Extruded AA6082 Alloy.* Trond Furu, Hans Erik Vatne. 2000, Materials Science Forum, Vols. 331-337, pp. 843-848.

[40] *On the Zener Drag.* E. Nes, N. Ryum and O. Hunder. 1, 1985, Acta Metallurgica, Vol. 33, pp. 11-22.

[41] *Five Decadesof the Zener Equation.* P. A. Manohar, M Ferry and T Chandra. 9, 1998, ISIJ International, Vol. 38, pp. 913-924.

[42] *The effect of solutes on grain boundary mobility during recrystallization and grain growth in some single-phase aluminium alloys.* Y. Huang, F.J. Humphreys. 2012, Materials Chemistry and Physics, Vol. 132, pp. 166-174.